J. Fluid Mech. (2002), *vol.* 453, *pp.* 345–369.
DOI: 10.1017/S002211200100698X Printed in the United Kingdom

Rayleigh–Bénard convection in liquid metal layers under the influence of a horizontal magnetic field

By ULRICH BURR[1] AND ULRICH MÜLLER[2]

[1]Eidgenössische Technische Hochschule Zürich, Institut für Hydromechanik und Wasserwirtschaft, ETH Hönggerberg, CH-8093 Zürich, Switzerland

[2]Forschungszentrum Karlsruhe GmbH, Institut für Kern- und Energietechnik, Postfach 3640, D-76021 Karlsruhe, Germany

(Received 28 September 2000 and in revised form 14 September 2001)

This article presents an analytical and experimental study of magnetohydrodynamic Rayleigh–Bénard convection in a large aspect ratio, 20 : 10 : 1, rectangular box. The test fluid is a eutectic sodium potassium $Na^{22}K^{78}$ alloy with a small Prandtl number of $Pr \approx 0.02$. The experimental setup covers Rayleigh numbers in the range $10^3 < Ra < 8 \times 10^4$ and Chandrasekhar numbers $0 \leqslant Q \leqslant 1.44 \times 10^6$ or Hartmann numbers $0 \leqslant M \leqslant 1200$, respectively.

When a horizontal magnetic field is imposed on a heated liquid metal layer, the electromagnetic forces give rise to a transition of the three-dimensional convective roll pattern into a quasi-two-dimensional flow pattern in such a way that convective rolls become more and more aligned with the magnetic field. A linear stability analysis based on two-dimensional model equations shows that the critical Rayleigh number for the onset of convection of quasi-two-dimensional flow is shifted to significantly higher values due to Hartmann braking at walls perpendicular to the magnetic field. This finding is experimentally confirmed by measured Nusselt numbers. Moreover, the experiments show that the convective heat transport at supercritical conditions is clearly diminished. Adjacent to the onset of convection there is a significant region of stationary convection with significant convective heat transfer before the flow proceeds to time-dependent convection. However, in spite of the Joule dissipation effect there is a certain range of magnetic field intensities where an enhanced heat transfer is observed. Estimates of the local isotropy properties of the flow by a four-element temperature probe demonstrate that the increase in convective heat transport is accompanied by the formation of strong non-isotropic time-dependent flow in the form of large-scale convective rolls aligned with the magnetic field which exhibit a simpler temporal structure compared to ordinary hydrodynamic flow and which are very effective for the convective heat transport.

1. Introduction

When a magnetic field is imposed on a heated liquid metal layer, Joule dissipation strongly damps the convective motions if three-dimensional convective flow patterns are present. This has already been demonstrated in our previous investigations of the effect of a purely vertical magnetic field on heat transfer (see Burr & Müller 2001). However, if a magnetic field is imposed in a purely horizontal direction and if the

electromagnetic forces are strong compared to inertial ones, the flow undergoes a reorganization towards two-dimensional convective rolls aligned with the magnetic field and with considerably less Joule dissipation. This effect has already been discovered by Chandrasekhar (1961) in his linear stability analysis of an infinitely extended horizontal layer heated from below. He states that for a magnetic field inclined towards the direction of gravity, convection at marginal stability will be manifested as longitudinal rolls aligned with the horizontal component of the magnetic field, whereas a delayed onset of convection results from the vertical component of the magnetic field only. Even for large supercritical conditions the two-dimensional structure of the flow is maintained as demonstrated in the experiments of Lehnert & Little (1956), Fauve, Laroche & Libchaber (1981) Fauve *et al.* (1984) and Kishida & Takeda (1994). The dynamics of the process are essentially the same as those for the formation of purely two-dimensional or quasi-two-dimensional magnetohydrodynamic (MHD) turbulence in duct flows and can be explained by applying the basic principles of MHD flow to single, isolated vortices. Davidson (1995) shows for the limiting case of high Reynolds numbers $Re = v_0 a/\nu$ and small magnetic Reynolds numbers $Rm = \mu\sigma v_0 a$ that the component of angular momentum aligned with the magnetic field is conserved, whereas components non-aligned with the magnetic field are removed on a fast time scale. The Lorentz force elongates vortices along the field lines and thereby Joule dissipation is continuously reduced. As a consequence, a purely two-dimensional flow is established, provided that this is consistent with the boundary conditions and that inertial forces are not destabilizing the flow. In purely two-dimensional flow the current density and with it electromagnetic forces vanish and the flow is governed by two-dimensional hydrodynamics (see Burr *et al.* 2000). However, a purely two-dimensional state can only be obtained in an infinite fluid domain. If the fluid is confined by walls perpendicular to the magnetic field, the vortices, i.e. the convective rolls, have to match the non-slip boundary condition at these so-called Hartmann walls and a quasi-two-dimensional flow develops. In figure 1(*a*) the geometry of Rayleigh–Bénard convection and the anticipated flow pattern of quasi-two-dimensional convective rolls is sketched. An electrically well conducting fluid (e.g. liquid metal) is confined between two horizontal walls which are separated by a height h and which are considered to be perfect thermal and electrical conductors. By heating the lower and cooling the upper wall a temperature difference ΔT is maintained parallel to the acceleration due to gravity $\boldsymbol{g}$ and if the temperature difference exceeds a critical value, a buoyant convective motion is established. A homogeneous magnetic field may be imposed on the layer in the horizontal x-direction. In the horizontal z-direction the layer is assumed to be of infinite extent whereas in the direction of the magnetic field the fluid domain is limited by two thin electrically conducting Hartmann walls separated by a distance $2b$, where s is the thickness of the wall material of electrical conductivity σ_W. Consistent with the common notation in MHD flows the horizontal walls aligned with the direction of the magnetic field and the adjacent boundary layers are called sidewalls and side layers, respectively.

In quasi-two-dimensional MHD flows the velocity distribution $\boldsymbol{v}(\boldsymbol{x})$ is uniform in the direction of the magnetic field over a core region that covers the major part of the fluid domain. At the Hartmann walls the core velocity matches the non-slip boundary condition by formation of thin Hartmann boundary layers. Figure 1(*b*) shows the anticipated current paths in a periodic sequence of counter-rotating convective vortices in the horizontal centreplane and in a vertical plane perpendicular to the magnetic field. Depending on the sense of rotation, electric currents $\boldsymbol{j}$ are induced radially out

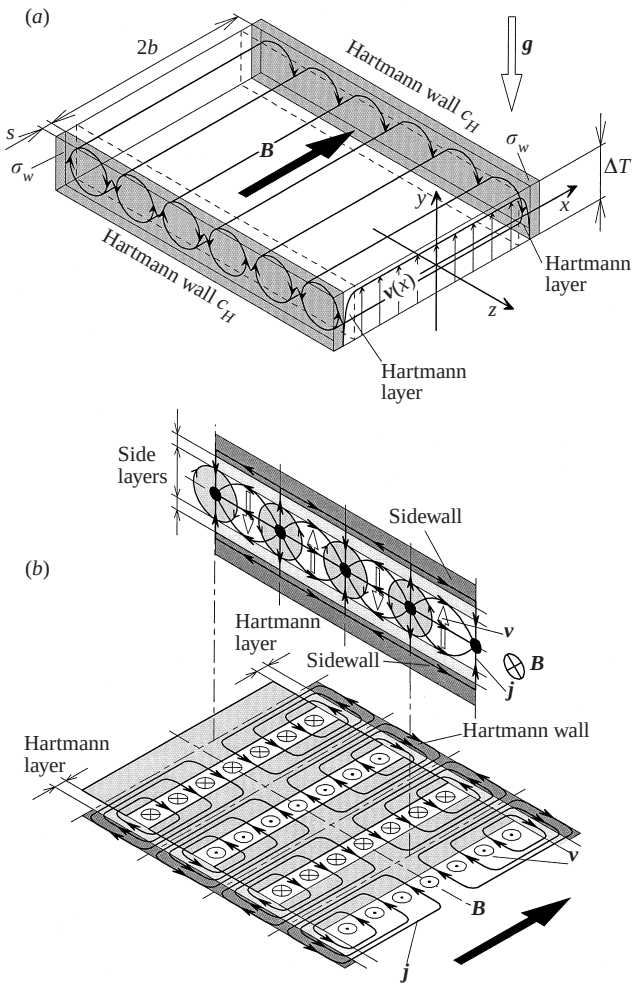

FIGURE 1. Quasi-two-dimensional magnetohydrodynamic flow at high magnetic fields in Rayleigh–Bénard convection. (*a*) Geometry and flow pattern of convective rolls aligned with the magnetic field. (*b*) Closure paths of the electric currents.

from or in towards the convective vortices, as it is seen from the vertical cut. Thus the centres of rotation of two adjacent vortices are connected by current paths through the fluid or via the electrically conducting sidewalls. Due to the reduced circulating velocity in the Hartmann boundary layer, the induced electric potential differences are smaller at the Hartmann walls. Therefore, the electric currents close along the direction of the magnetic field through the centre regions of two counter-rotating vortices via the Hartmann layers and the Hartmann walls, provided the latter are electrically conducting.

In the core region the Lorenz forces $\boldsymbol{F}_L = \boldsymbol{j} \times \boldsymbol{B}$ are directed opposite to the convective motions whereas at the Hartmann walls their direction is reversed and the fluid is accelerated. This renders the Hartmann layers very thin and thereby, together with conducting Hartmann walls, they govern the current density and with it the damping of velocity in the core region. The energy removed from the core region is dissipated by Joule dissipation in the Hartmann walls and by Joule and

viscous dissipation in the Hartmann layers. The dissipative effect of the Hartmann walls and layers is called Hartmann braking and is well known in duct flows (see e.g. Sommeria & Moreau 1982 and Bühler 1996). We shall see later (§4) that it delays the onset of convection which does not happen for horizontally infinite layers. Therefore, this study is focused on the role of Hartmann walls on the convective flow and the extension of established models, valid for duct flows, to the problem of magnetoconvective flows with strong external magnetic fields. The paper is organized as follows:

In §2 the general MHD equations, their scaling and the dimensionless numbers are presented. The model equations of quasi-two-dimensional natural convective flow are derived in §3. In §4 a linear stability analysis is performed. A brief outline of the experimental setup is given in §5 and in §6 experimental results are presented with an outline of general features, a discussion of integral flow properties and an investigation of the specific temporal structure of the flow. In §7 the results are summarized and some conclusions are drawn.

2. Governing equations and relevant dimensionless numbers

MHD flows for engineering conditions are described well by the limiting case of small magnetic Reynolds numbers $Rm \ll 1$ with $Rm = \mu\sigma v_0 a$ representing the ratio of the magnetic field induced by the fluid motion to the externally applied magnetic field. Here μ is the magnetic permeability, σ is the electrical conductivity of the fluid, v_0 a characteristic velocity and a a characteristic length. For this and the Bousinesq assumption the buoyant flow of a Newtonian fluid is governed by the following set of dimensionless equations:

mass, momentum and charge conservation

$$\nabla \cdot \boldsymbol{v} = 0, \tag{1}$$

$$\frac{1}{Pr}\left[\frac{\partial \boldsymbol{v}}{\partial t} + (\boldsymbol{v}\cdot\nabla)\boldsymbol{v}\right] = -\nabla p^* + \nabla^2 \boldsymbol{v} + RaT\boldsymbol{e}_y + Q\boldsymbol{j}\times\boldsymbol{B}, \tag{2}$$

$$\nabla \cdot \boldsymbol{j} = 0. \tag{3}$$

Ohm's law

$$\boldsymbol{j} = -\nabla\phi + \boldsymbol{v}\times\boldsymbol{B}; \tag{4}$$

heat transport equation

$$\frac{\partial T}{\partial t} + (\boldsymbol{v}\cdot\nabla)T = \nabla^2 T. \tag{5}$$

In these equations $\boldsymbol{x} = (x, y, z)$, $\boldsymbol{v} = (u, v, w)$, $\boldsymbol{j} = (j_x, j_y, j_z)$, $\boldsymbol{B} = (b_x, b_y, b_z)$, ϕ, t and T denote the dimensionless coordinates, velocity, current density, magnetic field, electric potential, time and temperature, obtained by introducing the scales h, $v_0 = \kappa/h$, $\sigma v_0 B$, B, hv_0B, $t_0 = h^2/\kappa$ and ΔT, where h is the height of the layer, v_0 a characteristic velocity, B the reference intensity of the applied magnetic field, t_0 a characteristic time scale (here the thermal diffusion time), and $\Delta T = T_b - T_t$ the temperature difference between the lower and the upper fluid–wall interface temperatures T_b and T_t. The thermal diffusivity $\kappa = \lambda/\rho c_p$ is defined from the thermal conductivity λ, the density ρ and the specific heat capacity c_p, $p^* = h^2(p + \rho g h)/(\rho\nu\kappa)$ is the dimensionless pressure with ν representing the kinematic viscosity and $\boldsymbol{e}_y$ is the unit vector directed opposite to the gravity vector of magnitude g.

MHD natural convective flow is characterized by three independent dimensionless groups: the Rayleigh number

$$Ra = \frac{\beta g \Delta T h^3}{\nu \kappa}, \tag{6}$$

where β is the cubic thermal expansion coefficient, the Prandtl number

$$Pr = \frac{\nu}{\kappa}, \tag{7}$$

and the Chandrasekhar number

$$Q = M^2 = \frac{B^2 h^2 \sigma}{\rho \nu}, \tag{8}$$

which is the square of he Hartmann number M commonly used in MHD duct flows.

In MHD flows the electrical properties of walls have significant influence. They are taken into account by the wall conductance ratio

$$c = \frac{\sigma_W s}{\sigma b}, \tag{9}$$

where σ_W is the electrical conductivity of the wall material, s is the thickness of the wall and b is the half-width of the flow region in the direction of the magnetic field. If $c \ll 1$, the thin wall condition (Walker 1981)

$$-c\nabla_t^2 \phi = \boldsymbol{j} \cdot \boldsymbol{n} \tag{10}$$

is valid, where $\boldsymbol{n}$ is the unit vector perpendicular to the wall and ∇_t^2 is the two-dimensional Laplace operator perpendicular to $\boldsymbol{n}$. We will see in the next section that for quasi-two-dimensional flow in high magnetic fields only the wall conductance ratio of the Hartmann walls c_H has significant influence on the flow. If three-dimensional flow patterns are present the wall conductance ratio of the sidewalls c_s may have an additional significant influence on the flow.

3. Formulation of two-dimensional equations

To describe quasi-two-dimensional MHD flow in ducts two-dimensional model equations have been derived by several authors (see e.g. Sommeria & Moreau 1982; Verron & Sommeria 1987; Bühler 1996). The basic idea of these model equations is to integrate the Hartmann braking effect at walls perpendicular to the magnetic field into a two-dimensional formulation of the flow in the core region. As quasi-two-dimensional natural convection has been found to occur in several experiments (see § 1) the formulation of two-dimensional model equations for natural convective flows seems justified. Moreover, buoyant flows have much longer time scales than duct flows and thus allow a fast formation of quasi-two-dimensionality out of a three-dimensional state.

Only a brief outline of the quasi-two-dimensional formulation of MHD flow will be given here with emphasis on the role of buoyant forces and the presence of walls aligned with the magnetic field. For a detailed formulation for non-buoyant flows see Bühler (1996).

By taking the curl of the momentum equation (2) the transport equation of vorticity $\boldsymbol{\Omega} = \nabla \times \boldsymbol{v}$ is obtained:

$$\partial_t \boldsymbol{\Omega} + (\boldsymbol{v} \cdot \nabla)\boldsymbol{\Omega} - (\boldsymbol{\Omega} \cdot \nabla)\boldsymbol{v} = Pr\nabla^2 \boldsymbol{\Omega} + RaPr\nabla \times (T\boldsymbol{e}_y) + QPr\partial_x \boldsymbol{j}. \tag{11}$$

The short forms ∂_t and ∂_x denote the partial derivatives with respect to t and x respectively or any other property. In a quasi-two-dimensional flow, with the magnetic field in the x-direction, the velocity field can be expressed by

$$u = 0, \quad v = -\partial_z \psi(y,z) f(x), \quad w = \partial_y \psi(y,z) f(x), \tag{12}$$

where $\psi(y,z)$ is a two-dimensional stream function defined as $v = -\partial_z \psi$ and $w = \partial_y \psi$ and $f(x)$ is a shape function that has to satisfy the non-slip conditions at the Hartmann walls $f(x = \pm b) = 0$ and the symmetry condition $\partial_x f(x = 0) = 0$; b is used in dimensionless form scaled with the layer height. In order to justify this form of the velocity field, the flow variables in the core region, denoted by a subscript c, must be uniform in the direction of the magnetic field and the thickness of the Hartmann layer has to be independent of the core variables to the main order of approximation. These two requirements are met if the electromagnetic forces dominate the momentum equation, i.e. if for very large values of Q (i.e. $Q \to \infty$)

$$Ra/Q \ll 1 \tag{13}$$

and generally also

$$PrQ \gg 1 \tag{14}$$

for the case of $Pr \ll 1$, considered here.† In this case equation (11) reveals a very weak variation of the electric current along the magnetic field, i.e. the order relation

$$\partial_x \boldsymbol{j}_c \simeq 0, \quad (Ra/Q, PrQ) \to 0 \tag{15}$$

holds. Taking the curl of equation (11) and introducing the curl of equation (4), we also obtain

$$\partial_{xx} \boldsymbol{v}_c \simeq 0, \quad (Ra/Q, PrQ) \to 0 \tag{16}$$

Using the symmetry conditions at $x = 0$ we obtain from equations (15) and (16) equivalent relations

$$\partial_x \phi_c \simeq 0 \tag{17}$$

and

$$u_c = \partial_x v_c = \partial_x w_c \simeq 0. \tag{18}$$

Equation (17) states that the electric potential in the core region does not vary along the magnetic field lines to the order Ra/Q and $(PrQ)^{-1}$. According to Ohm's law (equation (4)) this can only be satisfied if the current density in the direction towards the Hartmann layers remains small. This is satisfied well for a single vortex embedded in a fluid domain which is infinite in the directions perpendicular to the vortex axis. When sidewalls parallel to the magnetic field are present side layers are formed and due to their limited thickness the electric potential may vary significantly along the direction of the magnetic field, if the sidewalls are non- or only poorly electrically conducting. If we assume the sidewalls to be perfect electrical conductors, i.e. if $c_s \to \infty$ can be justified from equation (9), potential gradients in the boundary layer along these walls are equalized and the electric potential becomes uniform, consistent with equation (17). The electric currents enter the sidewalls and can close via the Hartman layers without an additional resistance and the dissipation remains governed by the quasi-two-dimensional damping effect. Therefore, perfectly conducting sidewalls strongly support the validity of this quasi-two-dimensional formulation. Moreover,

† The condition $PrQ \gg 1$ is not relevant for the linear stability analysis outlined in §4. It is stated here for the general nonlinear quasi-two-dimensional problem.

for the current paths suggested in figure 1(*b*) equation (17) is also satisfied for the case of poorly conducting or even insulating sidewalls since the electrical currents close along the direction of the magnetic field via the core regions of two counter-rotating vortices and therefore are not influenced by the presence of sidewalls. However, as the thickness of the side layers is larger at smaller magnetic fields the side layers may significantly influence the flow in the core region at small Chandrasekhar numbers.

With the above boundary conditions the shape function of the quasi-two-dimensional flow $f(x)$ is calculated as a solution of Hartmann's problem (see Bühler 1996) as

$$f = 1 - \exp[Q^{1/2}(x - b)]. \tag{19}$$

This relation shows that the Hartmann layers are very thin, $O(Q^{-1/2})$. Therefore deviations from a two-dimensional temperature field are removed on a fast time scale by heat diffusion along the x-direction (see figure 1*a*) and the temperature field becomes uniform along the magnetic field lines.† This justifies describing the temperature field in the core region by the two-dimensional heat transport equation in the form

$$\partial_t T + v\partial_y T + w\partial_z T = \nabla^2_{yz} T. \tag{20}$$

Consistent with the analysis for duct flows the equations of motion and for the electric currents are integrated in the x-direction by using the thin wall condition (10) for uniform conductivity of the Hartmann walls and the boundary and symmetry conditions $\partial_x f(x = b) = -Q^{1/2}$ and $\partial_x f(x = 0) = 0$. Thus, terms $O(Q^{-1})$ are neglected. Furthermore, the reduced mass flow rate in the Hartmann layers is neglected by the use of approximation $\int_0^b f(x)\mathrm{d}x = b$. The whole procedure finally results in a set of two-dimensional equations of the form

$$\frac{1}{Pr}[\partial_t \omega + \partial_y \psi \partial_z \omega - \partial_z \psi \partial_y \omega] = \nabla^2_{yz}\omega - Ra\partial_z T - \frac{\omega}{\tau}, \tag{21}$$

with

$$\frac{1}{\tau} = \frac{Q^{1/2}}{b} + \frac{Qc_H}{b + c_H} \tag{22}$$

and

$$\nabla^2_{yz}\phi = \frac{b}{b + c_H}\omega, \tag{23}$$

where $\omega = \partial_y w - \partial_z v$ is the component of vorticity aligned with the magnetic field. Together with equation (20) these expressions describe the quasi-two-dimensional natural convection flow in the core region. The influence of the magnetic field on the flow by the effect of Hartmann braking is given by the last term of equation (21). The similarity parameter τ is the dimensionless decay time of quasi-two-dimensional flow by Joule dissipation. For electrically insulating Hartmann walls ($c_H \to 0$) the damping effect shows the asymptotic limit $1/\tau \sim Q^{1/2}$ whereas for electrically well conducting Hartmann walls ($c_H \to \infty$) $1/\tau \sim Q$ determines the damping of vorticity. Equation (23) gives the relation between the electric potential and the vorticity in the core region.

† Next to distant sidewalls of a plane, finite heated layer there is always a small lateral region of the order of the layer height, where the overall convective flow is influenced by temperature inhomogeneities due to kinematic and thermal boundary conditions at the side walls. In our case, of an aspect ratio 1 : 10 : 20, these effects can be neglected with regard to the quasi-two-dimensional core region. For a detailed discussion see Wesfreid, *et al.* (1978).

Equations (20)–(23) are particularly useful to describe stationary flows because in this case the formation time for quasi-two-dimensionality need not be considered. Nevertheless, the conditions (13) and (14) must hold. Since the flow is buoyancy driven the condition $Ra/Q \ll 1$ is the most restrictive assumption to be satisfied. We will show in the next section that buoyant flow exists even in this limit.

4. Linear stability analysis

The presence of the magnetic damping term in equation (21) indicates a significant influence of Hartmann braking on the onset of convection. Considering a flow configuration such as sketched in figure 1 the critical Rayleigh number Ra_c for the onset of quasi-two-dimensional stationary convection is obtained from a linear stability analysis of the model equations derived in § 3. It is assumed that the horizontal boundaries are impermeable and perfect conductors for heat and currents.

Introducing flow variables as a sum of a basic state denoted by subscript 0 and a disturbance denoted by prime, e.g. $\psi = \psi_0 + \varepsilon\psi'$ where ε is a small parameter, the governing equations of quasi-two-dimensional flow (20)–(23) are linearized by neglecting terms $O(\varepsilon^2)$. As the state of pure heat conduction is defined by $T_0 = -y$ and $\psi_0 = 0$, the disturbance of the temperature field in the linearized vorticity equation is eliminated and we obtain

$$0 = \nabla^6_{yz}\psi' - Ra\partial_{zz}\psi' - \frac{1}{\tau}\nabla^4_{yz}\psi'. \tag{24}$$

For a layer infinitely extended in the z-direction a periodic Ansatz of the form

$$\psi'(y, z) = \psi'(y)\exp(\mathrm{i}az) \tag{25}$$

can be chosen, where a is the horizontal wavenumber. Introducing (25) into equation (24) we obtain the linearized ordinary differential equation

$$(\mathrm{d}_{yy} - a^2)^3\psi'(y) - \frac{1}{\tau}(\mathrm{d}_{yy} - a^2)^2\psi'(y) = -Raa^2\psi'(y) \tag{26}$$

which defines the marginal state for the onset of convection as a stationary motion. The additional stiffness introduced by Joule dissipation of quasi-two-dimensional flow is represented by the second term on the left-hand side of equation (26).

If we assume for simplicity that both horizontal boundaries are free the basic odd mode

$$\psi(y) = \cos(\pi y) \tag{27}$$

which satisfies slip conditions at the boundaries $y = 0$ and $y = 1$ can be choosen as a solution in the interval $0 < y < 1$. Inserting this mode in equation (26) gives a solvability condition $F(Ra, a) = 0$ which results in the critical wavenumber

$$a_c = \frac{\pi}{2}\sqrt{\sqrt{\xi^2 + 8\xi} - \xi}, \quad \xi = 1 + \frac{1}{\pi^2\tau}, \tag{28}$$

and the critical Rayleigh number

$$Ra_c = \frac{(\pi^2 + a_c^2)^3 + 1/\tau(\pi^2 + a_c^2)^2}{a_c^2} \tag{29}$$

for onset of convection. In figures 2(a) and 2(b) the critical wavenumber and the corresponding critical Rayleigh number are plotted versus the decay time $1/\tau$ of

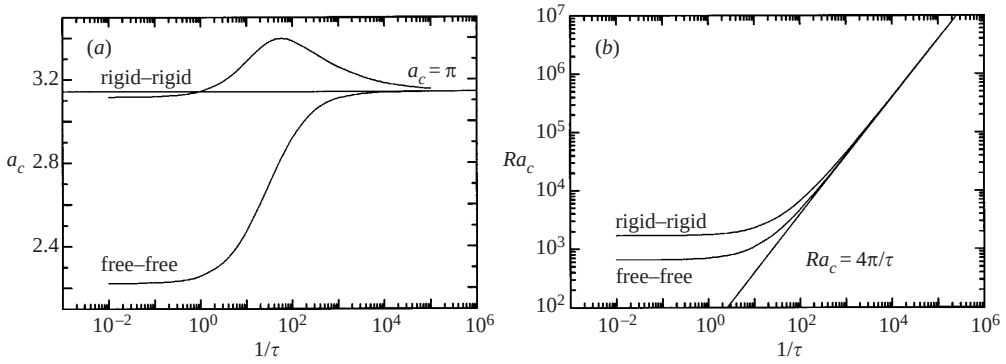

FIGURE 2. (*a*) Critical wavenumbers a_c and (*b*) critical Rayleigh numbers Ra_c for the onset of stationary quasi-two-dimensional convection in the pressence of Hartmann walls perpendicular to the magnetic field. The influence of the magnetic field is expressed by the inverse of the dimensionless decay time $1/\tau = Q^{1/2}/b + Qc_H/(b + c_H)$. The curves labelled free–free represent values obtained for slip conditions at both horizontall walls whereas curves labelled rigid–rigid represent values obtained for non-slip conditions at both horizontal walls. The curves $a_c = \pi$ and $Ra_c = 4\pi^2/\tau$ represent the asymptotic case of inviscid flow.

quasi-two-dimensional flow. The critical wave number increases from the value for purely hydrodynamic flow $a_c(1/\tau \to 0) = \pi/2^{1/2}$ continuously to the asymptotic value at high electromagnetic damping $a_c(1/\tau \to \infty) = \pi$. In the same way, the critical Rayleigh number increases monotonically from $Ra_c(1/\tau \to 0) = 27\pi^4/4$ and finally approaches a linear asymptotic law. This asymptotic behaviour can be derived by neglecting the effect of viscous friction, described by the first term in equation (26). Since $a_c(1/\tau \to \infty) = \pi$ we obtain from (29)

$$Ra_c = \frac{4\pi^2}{\tau}, \tag{30}$$

which is consistent with the findings of Horton & Rogers (1945) and Lapwood (1948) for convection in a porous medium where friction is accounted for by Darcy's law only.

If both horizontal boundaries are rigid and non-slip conditions hold, the critical values are obtained by expanding $\psi'(y)$ into a Fourier series of the form

$$\psi(y) = \sum_m A_m \cos[(2m+1)\pi y] \tag{31}$$

and solving equation (26) by a Galerkin method. Results of this procedure are also plotted in figures 2(*a*) and 2(*b*). The critical Rayleigh numbers increase from the value at hydrodynamic flow $Ra_c(1/\tau \to 0) = 1708$ and match at large $1/\tau$ the asymptotic behaviour of inviscid flow. The critical wave numbers exhibit an unexpected behaviour. The values first increase from the limiting value of purely hydrodynamic flow $a_c(1/\tau \to 0) = 3.117$, develop a maximum value of about $a_c \approx 3.4$ at $1/\tau \approx 60$, and then decrease for increasing magnetic field intensities to the asymptotic value of the inviscid case $a_c = \pi$.

5. Experimental setup and performance

A detailed description of the test section is given by Burr & Müller (2001). The test apparatus provides a confined liquid metal layer of large aspect ratio 1 : 10 : 20 and

a height of $h = 20\,\text{mm}$. Eutectic sodium-potassium alloy $Na^{22}K^{78}$, with 22% weight sodium and 78% weight potassium, was chosen as a test fluid. The temperature-dependent thermophysical properties are calculated based on fitting curves derived from data taken from O'Donnell, Papanicolaou & Reed (1989), Lyon (1952) and Foust (1972). Due to technical peculiarities of the experimental setup the mean temperature of the test fluid increases with increasing Rayleigh numbers. Moreover the Prandtl number varies in the range $0.017 < Pr < 0.021$ because of the temperature dependence of the physical properties. The Hartmann walls as well as the side walls aligned with the direction of the magnetic field are 1.5 mm thick stainless steel sheets. As the thermal conductivity of stainless steel is even lower than the thermal conductivity of NaK the vertical walls may be considered as isothermal and do not impose a linear temperature gradient on the fluid. With the electrical conductivities $\sigma_{ss} = 1.37 \times 10^6\,\Omega^{-1}\,\text{m}^{-1}$ and $\sigma = 2.47 \times 10^6\,\Omega^{-1}\,\text{m}^{-1}$ of stainless steel and NaK we obtain from equation (9) the small wall conductance ratio $c_H = 4.15 \times 10^{-3}$ of the Hartmann and the vertical sidewalls. Both horizontal walls are copper plates of 20 mm thickness and with the electrical conductivity $\sigma_{Cu} = 5.8 \times 10^7\,\Omega^{-1}\,\text{m}^{-1}$ of copper we obtain from equation (9) $c_S = 4.5$. Therefore the horizontal sidewalls meet to a good approximation the requirements of perfect thermal and electrical conductivity made in §§ 3 and 4.

The lower copper plate is electrically heated with a maximum power of $P \approx 11\,\text{kW}$ which results in Rayleigh numbers up to $Ra \approx 8 \times 10^4$. The test section is placed into the magnetic bore of a superconducting solenoid magnet which generates a horizontal magnetic field of up to 3.5 T and a homogeneity better than $\mp 4\%$. In this investigation tests were conducted only in the range of Chandrasekhar numbers $0 \leqslant Q \leqslant 1.44 \times 10^6$ or Hartmann numbers $0 \leqslant M \leqslant 1200$.

In figure 3 the geometry and instrumentations of the experimental setup are shown. The longer side of the test section is orientated parallel to the magnetic field $\boldsymbol{B}$. The temperature difference across the layer $\Delta T = T_b - T_t$ and the mean temperature of the fluid $T_m = (T_b + T_t)/2$ are evaluated from the five temperatures $T_{i,j}$ in each wall as a spatial and temporal average. The magnitude of the heat flux q supplied to the layer is known from the measurement of the electrical heating power. With known q the convective heat transport is expressed by the Nusselt number

$$Nu = \frac{q}{\lambda \Delta T / h}. \tag{32}$$

Physical properties as well as characteristic numbers are evaluated as temporal mean values only and therefore averaging is not indicated further.

The measurement of local time-dependent properties is facilitated by a four-element temperature probe which can sense the fluctuating parts T'_P of temperature T_P and $\nabla T'_P$ of the temperature gradient $\nabla T_P = (\partial_x T_P, \partial_y T_P, \partial_z T_P)$. The latter measurement is facilitated by a non-coplanar arrangement of four thermocouples each of 0.25 mm diameter (for details see Burr & Müller 2001).

As a measure for the intensity of the temperature fluctuations the variance of the temperature

$$\overline{T'^2_P} = \frac{1}{t_m} \int_0^{t_m} T'^2_P \mathrm{d}t, \tag{33}$$

is evaluated, where t_m is a sufficiently long time interval. An estimate of the integral

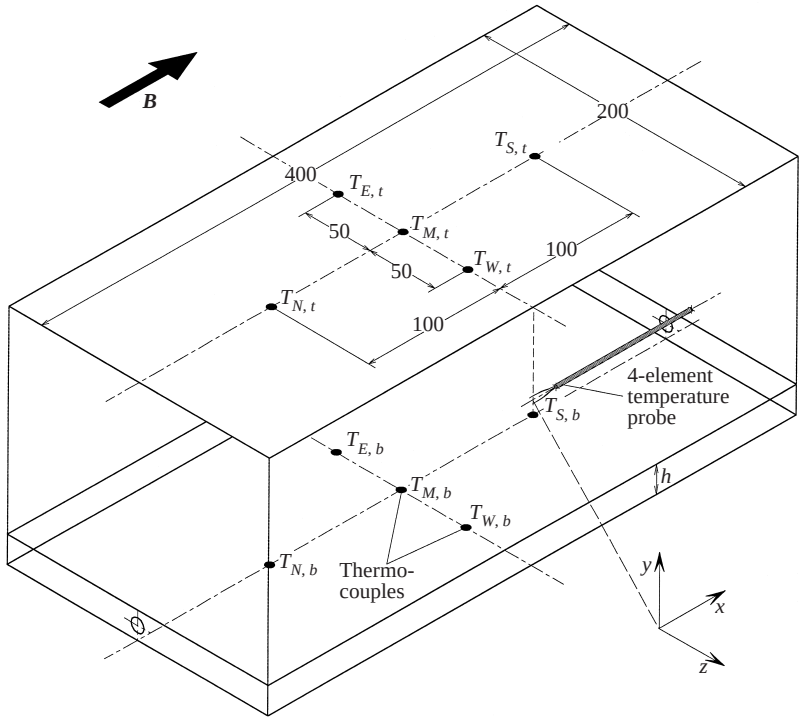

FIGURE 3. Instrumentation and geometry of the heat transfer test facility. Five Cu–CuNi thermo-couples are placed at the upper and the lower fluid–wall interface to obtain wall temperatures $T_{i,j}$. Local, time-dependent flow quantities are obtained from a four-element temperature probe placed in the middle of the fluid layer. All lengths are given in mm.

time scale τ_I of the flow is obtained from

$$\tau_I = \frac{2\pi}{t_0} \int_0^{t_I} A(t)\mathrm{d}t, \tag{34}$$

where $A(t)$ is the autocorrelation function of the temperature signal normalized with $\overline{T_P'^2}$, t_I the time shift where $A(t)$ becomes zero, and $t_0 = h^2/\kappa \approx 15.5\,\mathrm{s}$ is the thermal diffusion time that renders τ_I dimensionless.

From the ratio between the variances of the horizontal temperature gradients $\overline{(\partial_x T_P)'^2}$ and $\overline{(\partial_z T_P)'^2}$ the horizontal isotropy coefficient

$$A_{xz} = \frac{\overline{(\partial_x T_P)'^2}}{\overline{(\partial_z T_P)'^2}} \tag{35}$$

is defined as a measure for the local isotropy property of the flow. If A_{xz} approaches unity, the flow may be called horizontally isotropic. This situation can be expected for a heated infinite layer in the case of no electrodynamic forces. If a quasi-two-dimensional, time-dependent flow is established under the effect of a strong horizontal magnetic field, the quasi-two-dimensional velocity field will render the temperature distribution quasi-two-dimensional as well and therefore $\partial_x T_P' \approx 0$ holds in the core region. Thus, for quasi-two-dimensional flow A_{xz} approaches zero and it is reasonable to expect the trend towards a two-dimensional velocity field from decreasing values of the horizontal isotropy coefficient.

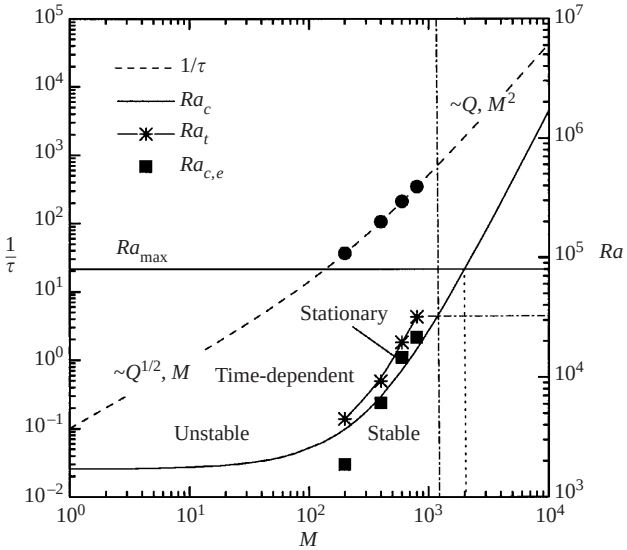

FIGURE 4. Critical Rayleigh number Ra_c and the magnetic damping parameter $1/\tau$ obtained from a stability analysis (§ 4) of the two-dimensional-model equation (§ 3) as a function of the Hartmann number M. The dots mark the experimentally realized Hartmann numbers $M = 200$, 400, 600 and 800. The experimentaly obtained critical Rayleigh numbers for onset of convection as stationary motion $Ra_{c,e}$ and for onset of time-dependent flow Ra_t are plotted as squares and stars.

6. Experimental results

6.1. *General observations*

The range of experimentally feasible convection states and the magnetic damping effect of the test chamber is displayed in figure 4, where the critical Rayleigh number Ra_c and the magnetic damping parameter $1/\tau$ are plotted as a function of the square root of the Chandrasekhar number $Q^{1/2}$, i.e. the Hartmann number M that will, for convenience, be used in the following to denote the intensity of the magnetic field. The other curves are the result of the stability analysis of § 4 and the graph for the magnetic damping parameter $1/\tau$ results from the formulation of the two-dimensional-model equation (21) in § 3. The highest experimentally achievable Rayleigh number $Ra_{\max} \approx 8 \times 10^4$ is marked in figure 4 by a horizontal straight line and the feasible supercritical convective state lies between the curve of marginal stability at the lower side and the maximum Rayleigh number $Ra_{\max}$ from above. The graph in figure 4 will be used later for the discussion of the experimental results.

To investigate the basic features of the natural convective flow under the influence of a horizontal magnetic field we apply in a first series of experiments a fixed heat flux of magnitude $q = 2.8 \times 10^4\,\mathrm{W\,cm^{-2}}$ to the layer and increase the magnetic field from the pure hydrodynamic case given by $M = 0$ up to $M = 1200$ and wait for the test facility to overcome transient effects before the measurements are started. We choose as typical integral flow quantities to characterize the MHD natural convection the heat transfer in terms of Nusselt number Nu, the mean driving temperature difference in terms of Rayleigh number Ra, the variances of temperature fluctuations $\overline{T_P'^2}$ recorded by the probe, the integral time scale τ_I and the horizontal isotropy coefficient A_{xz}. In figure 5 these characteristic integral flow properties are plotted versus the Hartmann number M.

When the external magnetic field is applied to the heated liquid metal layer and

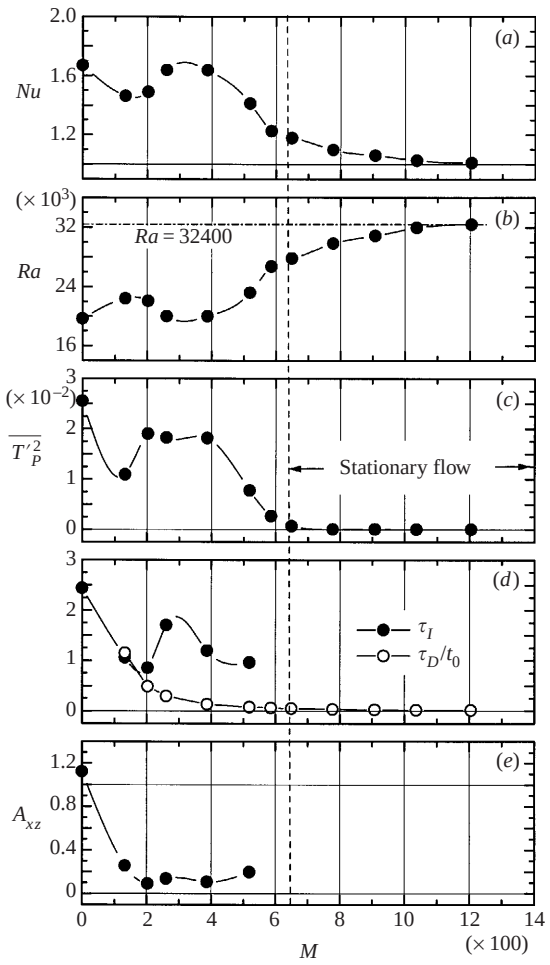

FIGURE 5. Influence of increasing the Hartmann number M on relevant integral flow quantities at constant heat flux $q = 2.8 \times 10^4\,\mathrm{W\,m^{-2}}$. ($a$) Nusselt numbers Nu. (b) Rayleigh numbers Ra. (c) Variances of the temperature $\overline{T_P'^2}$ in the fluid measured by the probe. (d) Integral time scale of the flow τ_I and diffusion time of vorticity along magnetic field lines τ_D scaled with the thermal diffusion time t_0. (e) Horizontal isotropy coefficient A_{xz}.

gradually increased to large intensities the convective heat transfer generally decreases because of the increased Joule dissipation at higher magnetic field intensities. As a consequence the Nusselt numbers plotted in figure 5(a) decrease asymptotically for strong magnetic fields until, in the present case for $M \approx 1200$, the value $Nu = 1$ is achieved indicating a state of pure heat conduction. However, the Nusselt number does not decrease monotonically for increasing Hartmann numbers. In an intermediate range between $M \approx 200$ and $M \approx 400$ the convective heat transfer increases and the Nusselt number curve reaches a maximum.

With a constant heat flux the changes in the convective heat transfer also affect the Rayleigh numbers as seen in figure 5(b). For the state of pure heat conduction with $Nu = 1$ the terminal Rayleigh number $Ra = 32\,400$ is obtained. This value is indicated in figure 5(b) by a horizontal dash-dotted line and in figure 4 by the vertical

dash-dotted line. In figure 4 it intersects the curve of the critical Rayleigh number at $M \approx 1180$. This is in good agreement with the results of the linear stability analysis.

The intensity of temperature fluctuations is characterized by the variances of the temperature fluctuations $\overline{T_P'^2}$ of the probe as shown in figure 5(c). It is affected by the magnetic field in a similar way as the Nusselt number. Beyond $M \approx 700$, indicated in figure 5(a–e) by the vertical dashed line, the variance virtually vanishes and the originally time-dependent flow undergoes a transition to laminar stationary convection which still allows a significant convective heat transfer with $Nu > 1$ in the region of stationary convection.

The evaluated integral time scale τ_I is plotted in figure 5(d). The graph shows that the dynamics of the flow become generally faster under the influence of the magnetic field as the time scale is reduced.

The horizontal isotropy coefficient A_{xz} is plotted in figure 5(e). It may explain the non-monotonic behaviour of Rayleigh and Nusselt numbers as well as the intensity of temperature fluctuations in the time-dependent region as a consequence of a significant change in the local isotropy properties of the flow. With a relatively moderate magnetic field corresponding to $M \approx 130$ the horizontal isotropy coefficient A_{xz} immediately decreases to a very small value of about $A_{xz} \approx 0.1$ showing that the flow becomes more and more two-dimensional, at least locally, in the sense that convective flow structures become aligned with the magnetic field. Because of the growing two-dimensional character of the flow, Joule dissipation is reduced compared to three-dimensional flow and higher convective velocities may occur with higher convective heat transport and stronger temperature fluctuations. This process seems to be most significant for Hartmann numbers around $M \approx 300$ where the local maximum of the Nusselt number curve is observed. The slight increase of A_{xz} in the range $M \gtrsim 400$ results from a relatively higher noise level for small temperature fluctuations.

The quasi-two-dimensional character of the time-dependent convection, as suggested by the isotropy coefficient A_{xz} in figure 5(e), can further be reasoned from the following scale considerations. The integral time scale as plotted in figure 5(d) is assumed to be an indicator of a transport of temperature inhomogeneities over a distance of the order of the layer height, $O(h)$. It is seen from figure 5(d) that τ_I is $O(1)$, i.e. it is comparable with the thermal diffusion time scale t_0 during which a temperature disturbance loses its identity by thermal diffusion. For turbulent MHD flow Sommeria & Moreau (1982) describe the propagation of vorticity in the direction of the magnetic field by a diffusion process based on a diffusivity $\alpha = \sigma B^2 l_\perp^2/\rho$, where $l_\perp$ is a typical length scale perpendicular to the magnetic field which in our case is measured by the layer height h. The related diffusion time scale for an equalization of velocities in two planes of distance d apart and perpendicular to the magnetic field is then given by

$$\tau_D = \frac{\rho}{\sigma B^2}\frac{d^2}{l_\perp^2}. \tag{36}$$

This diffusion time scale was evaluated assuming for the relevant experimental length scales $l_\perp = h$ and $d = 2b$, and was normalized by the thermal diffusion time t_0. The data are plotted in figure 5 (d) together with those for the integral time scale τ_I. The graph shows that the diffusion time scale for the propagation of vorticity along the magnetic field lines becomes smaller than the integral time scale for the transportation of temperature perturbations for Hartmann numbers $M \gtrsim 200$. This may explain why a quasi-two-dimensional convective flow can be established under

M	$Q = M^2$	B [T]	$1/\tau$	Ra_c	Ra_c/Q	$Ra_{c,e}$
0	0	0	0	1708	∞	2050
200	4.0×10^4	0.15	36.6	3.65×10^3	0.091	1870
400	1.6×10^5	0.29	106.4	6.97×10^3	0.044	6150
600	3.6×10^5	0.43	209.5	1.14×10^4	0.032	14600
800	6.4×10^5	0.58	345.7	1.71×10^4	0.027	21400

TABLE 1. Hartmann numbers M, Chandrasekhar numbers Q, approximate magnitudes of the applied magnetic field B, magnetic damping parameter $1/\tau$, critical Rayleigh number for the onset of convection obtained from quasi-two-dimensional theory Ra_c, the ratio Ra_c/Q and experimentally determined values for the onset of convection $Ra_{c,e}$.

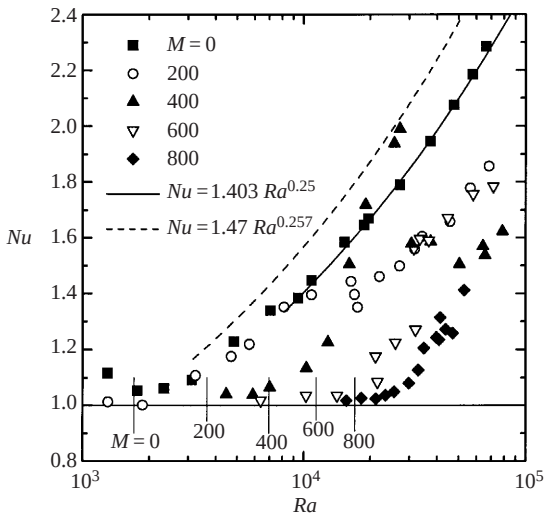

FIGURE 6. Nusselt numbers Nu versus Rayleigh numbers Ra for OHD flow ($M = 0$) and MHD flows for $M = 200$, 400, 600 and 800. The vertical solid lines indicate the critical Rayleigh numbers Ra_c for the onset of convection calculated using the linear stability analysis in § 4.

the influence of a magnetic field in spite of the homogenizing effect of temperature fluctuations.

6.2. *Integral heat transfer and onset of convection*

The convective heat transfer is investigated in a two parameter range of Rayleigh and Chandrasekhar numbers. The heat flux applied to the layer is varied in the range $1.26 \times 10^3 \leqslant q \leqslant 1.25 \times 10^5\ \mathrm{W\,m^2}$ to cover the widest attainable range of Rayleigh numbers $10^3 < Ra < 8 \times 10^4$. The effects of five Hartmann numbers, including ordinary hydrodynamic (OHD) flow with $M = 0$ are investigated. The Hartmann numbers M, the Chandrasekhar numbers Q, the approximate magnitudes of the magnetic field B and the corresponding magnetic damping parameter $1/\tau$ are listed in table 1. The particular Hartmann numbers are indicated in figure 4 as circles. Furthermore, the critical Rayleigh numbers for the onset of convection for two rigid walls (see figure 2) Ra_c and the ratio Ra_c/Q are given.

In figure 6 the Nusselt numbers for the whole test matrix are plotted versus the Rayleigh number. Here, the critical Rayleigh numbers Ra_c as calculated using the linear stability analysis of § 4 for the onset of convection are indicated by vertical solid

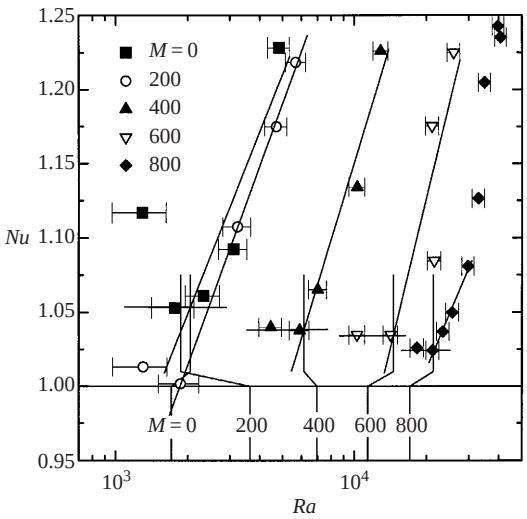

FIGURE 7. Nusselt numbers Nu versus Rayleigh numbers Ra at marginally supercritical conditions. The symbols represent measurements for OHD flow ($M = 0$) and MHD flows for $M = 200$, 400, 600 and 800. The vertical solid lines at $1.01 < Nu < 1.075$ display the experimentally determined critical Rayleigh numbers for the onset of convection $Ra_{c,e}$ which are connected to corresponding vertical lines for $Nu < 1$ which display the critical Rayleigh numbers Ra_c for the onset of convection as calculated using the linear stability analysis of § 4.

lines. The results for the different Hartmann numbers are obtained by systematically decreasing the applied heat flux. Additionally the magnetic field was always adjusted to its final value by decreasing it from higher values. Some indications of hysteresis effects were observed but a systematic investigation was not performed. For OHD flow ($M = 0$), the Nusselt numbers rise above the conductive level $Nu = 1$ beyond the critical value of the Rayleigh number for onset of convection $Ra_c = 1708$ and thereby indicate the onset of convective motions and the related heat transport. As the Nusselt numbers of MHD flow level off at much higher Rayleigh numbers, there is a clear increase of the critical Rayleigh number by the magnetic field. In order to derive critical Rayleigh numbers from the experimental data, the Nusselt numbers at marginally supercritical conditions are replotted in figure 7. Due to uncertainties concerning the material properties used for the evaluation (see Burr & Müller 2001), the Nusselt numbers do not approach the value $Nu = 1$, as the Rayleigh numbers are decreased below critical conditions. Therefore, stable conditions corresponding to the basic preconvective state are suggested where the Nusselt numbers maintain a constant value on decreasing the Rayleigh number as indicated by the horizontal lines ($Nu > 1$). We observe that except for the smallest Rayleigh number in OHD flow the error in determining the Nusselt numbers at subcritical Rayleigh numbers is less than 6%. The horizontal error bars in figure 7 represent the uncertainty in determining the Rayleigh number. They are determined from assuming an uncertainty of 5% in the physical properties and a measurement error in the temperature difference of 0.2 K when calculating the Rayleigh number. The critical Rayleigh numbers $Ra_{c,e}$ are obtained from the intersection points of linear fitting curves to the marginally supercritical Rayleigh numbers, plotted as straight lines, with the corresponding horizontal lines indicating the basic state of conduction. The values thus obtained are displayed in the region $1.075 < N < 1.01$ as vertical solid lines. They are connected to

the corresponding vertical lines in the region $Nu < 1$ which show the critical Rayleigh numbers obtained from the stability analysis. The $Ra_{c,e}$ values are also compiled in table 1 and plotted in figure 4 as squares. For Hartmann number $M = 400$ and higher the experimentally determined critical Rayleigh numbers agree reasonably well with the predictions of the stability analysis of the quasi-two-dimensional theory and so confirm the significance of the Hartmann walls as a source of increased Joule dissipation. However, for small Hartmann numbers, i.e. $M \simeq 200$, of the theoretical value of Ra_c is significantly greater than the observed one. Since even for $M = 200$ the ratio Ra/Q is still small, i.e. $Ra_c/Q \approx 0.1$ (see table 1), this discrepancy cannot be explained by the violation of assumption (13) made in § 3 for the validity of the two-dimensional model equations. It might arise from an effect of side layers which is not taken into account by the linear stability analysis. For small values of $M \lesssim 200$ the total thickness of the side layers is of the order of the layer height and this may significantly reduce the effective region of the Hartmann layers at the vertical walls. Thereby the overall Joule dissipation is reduced in the experiment, which results in lower critical Rayleigh numbers.

For the high values Ra plotted in figure 6 the Nusselt number data for OHD flow at $Q = 0$ can be fitted by the scaling law $Nu = 1.403 \times Ra^{0.250 \pm 0.004}$ valid for $10^4 > Ra > 10^5$. The exponent is in agreement with the findings for Rayleigh–Bénard convection in a layer of mercury with $Pr \approx 0.025$ by Rossby (1969) who derived from his measurements $Nu = 0.147 \times Ra^{0.257 \pm 0.004}$ (dotted line in figure 6). However, although the Prandtl number of NaK is similar to that of mercury, the Nusselt numbers in this experiment are determined as generally lower, which might be a further indication of the uncertainties concerning the material properties used for the evaluation.

When a magnetic field is applied to the liquid layer the behaviour of the Nusselt numbers changes significantly. For a magnetic field corresponding to $M = 200$ the Nusselt numbers increase at first as for OHD flow up to $Ra \approx 10^4$ and Joule dissipation seems to have no effect yet on the convective heat transport although the intensity of the applied magnetic field is not small. At a Rayleigh number of about $Ra \approx 10^4$ the Nusselt number curve forms an intermediate plateau and thus shows that starting from this value the convective heat transfer is significantly inhibited by the magnetic field. Within the plateau region several states of heat transfer characterized by different combinations of Ra and Nu are observed for the same applied heat flux but different start-up conditions. Similar observations have been made recently in other Rayleigh–Bénard convection experiments with different external constraints (see e.g. Horanyi, Krebs & Müller 1999). The different states for the same set of external control parameters may be explained by variations in the convective flow pattern. Beyond $Ra = 5 \times 10^4$ the Nusselt numbers steeply increase again but remain well below the values for OHD convection. For the higher Hartmann number $M = 400$ the onset of convection is observed to be significantly shifted to higher Rayleigh numbers. Beyond the critical Rayleigh number the Nusselt number increases steeply and overshoots even the values obtained for OHD convection. However, at $Ra \approx 3.0 \times 10^4$ the convective heat transfer suddenly collapses to a much lower level and does not recover within the range of Rayleigh numbers investigated here. This unusual behaviour of the convective heat transfer is correlated with significant changes in the convective flow structure, which may be concluded from the time series of the local dimensionless temperature fluctuations T'_P measured by the probe and presented in figure 11. This and further details of the temporal dynamics of the natural convection will be discussed in § 6.3. For even higher Hartmann numbers

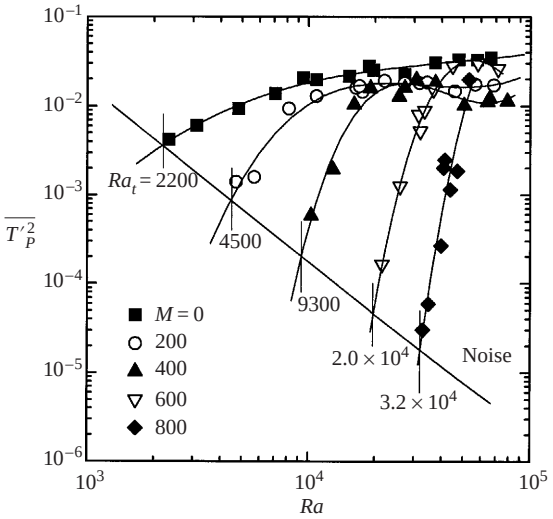

FIGURE 8. Variances of temperature $\overline{T_P'^2}$ recorded by the probe for OHD flow and MHD flows at different Hartmann numbers M. The critical Rayleigh numbers for the onset of time-dependent flow Ra_t are determined from the crosspoint of the fitting curves with the noise level.

M the Nusselt numbers exhibit the same behaviour as OHD convection, namely a monotonic increase with increasing Rayleigh numbers. The most remarkable feature of this heat transfer system is the heat transfer enhancement under the influence of an external horizontal magnetic field of moderate intensity which conforms with the local maximum of the Nusselt number in figure 5(a).

6.3. *Temporal structures*

From the linear stability analysis of §4 it can be shown that the convection starts as a stationary flow. Oscillatory convection originates from this state as a secondary bifurcation. The marginal conditions for this transition are investigated experimentally here by using the variances of the temperature fluctuations $\overline{T_P'^2}$ recorded by the probe as a measure of time dependence. In figure 8 the variances of all tests are plotted versus the Rayleigh number. Additionally a curve indicating the noise level, determined separately by thermally neutral instrumentation tests, scaling as Ra^{-2} is displayed in the same figure. The points of intersection between the fitting curves of measured variances and the noise level curve are taken as the experimentally determined condition for the onset of time-dependent oscillatory flow characterized by a second critical Rayleigh number Ra_t. These data points are plotted together with their fitting curve on the stability map of figure 4. Between this fitting curve and the curve of marginal stability an area of steady convection can be identified which generalizes the previous finding of figures 5(b) and 5(c), namely the occurrence of significant convective heat transfer in a range of high Hartmann number where temporal fluctuations are suppressed by Joule and viscous dissipation. Above Ra_t a strong increase of this measure to a saturation level with increasing Rayleigh numbers can be observed for all Hartmann numbers. The saturation level of the variances is highest for the OHD flow ($M = 0$).

The temporal behaviour beyond the second critical Rayleigh number Ra_t may be characterized by the integral time scale τ_I as defined in equation (34). This time scale is evaluated and displayed in figure 9 as a function of a reduced Rayleigh

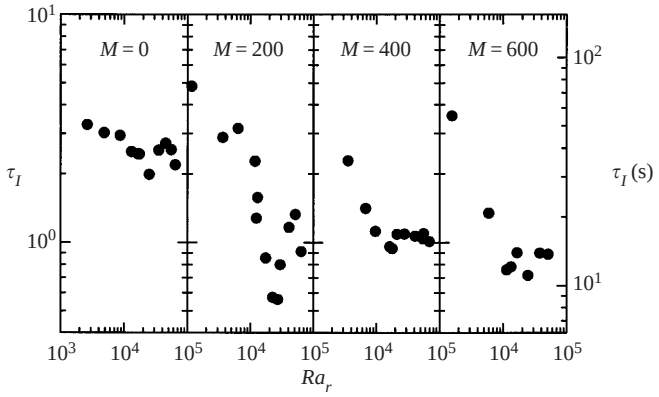

FIGURE 9. Integral time scales τ_I defined from equation (34) for Hartmann numbers $M = 0$, 200, 400 and 600 versus the reduced Rayleigh number $Ra_r = Ra - Ra_t$ where Ra_t is obtained from the experimental results in figure 8.

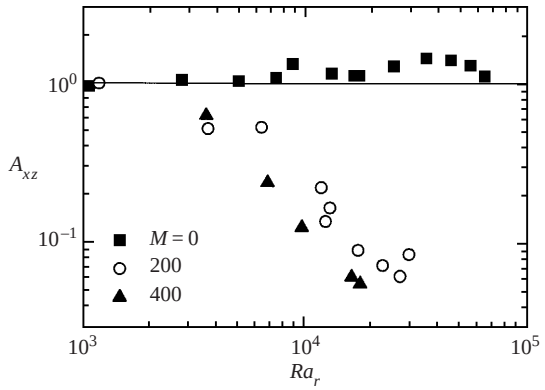

FIGURE 10. Horizontal isotropy coefficent A_{xz} plotted versus a reduced Rayleigh number $Ra_r = Ra - Ra_t$ for Hartmann numbers $M = 0$, 200 and 400.

number $Ra_r = Ra - Ra_t$. The graph shows that for increasing Rayleigh numbers and more strongly under the influence of an external magnetic field the integral time scale decreases, i.e. the fluctuation frequency increases. This observation is in agreement with findings of Fauve *et al.* (1981) who report an increase of the oscillation frequency with increasing Rayleigh numbers in their convection experiment under the ordering effect of a horizontal magnetic field. They suggest that the increase of the oscillatory instability frequency is associated with the suppression of the three-dimensional oscillatory instability. The energy thus released is transferred to a higher roll circulation velocity that results in faster dynamics of the flow.

Valuable information on the spatial structure of the time-dependent eddies is obtained from the horizontal isotropy coefficients A_{xz} plotted in figure 10 for OHD flow $M = 0$ and the strong time-dependent MHD flows at Hartmann numbers $M = 200$ and 400. In OHD flow values of approximately unity indicate horizontal isotropy of the flow. In MHD flow the horizontal isotropy coefficients are significantly smaller than for OHD flow in the region of large Ra_r and are further decreased from higher Chandrasekhar numbers consistent with the concept of enhanced non-isotropy at higher magnetic fields.

The temporal dynamics of Rayleigh–Bénard convection in a box of small aspect

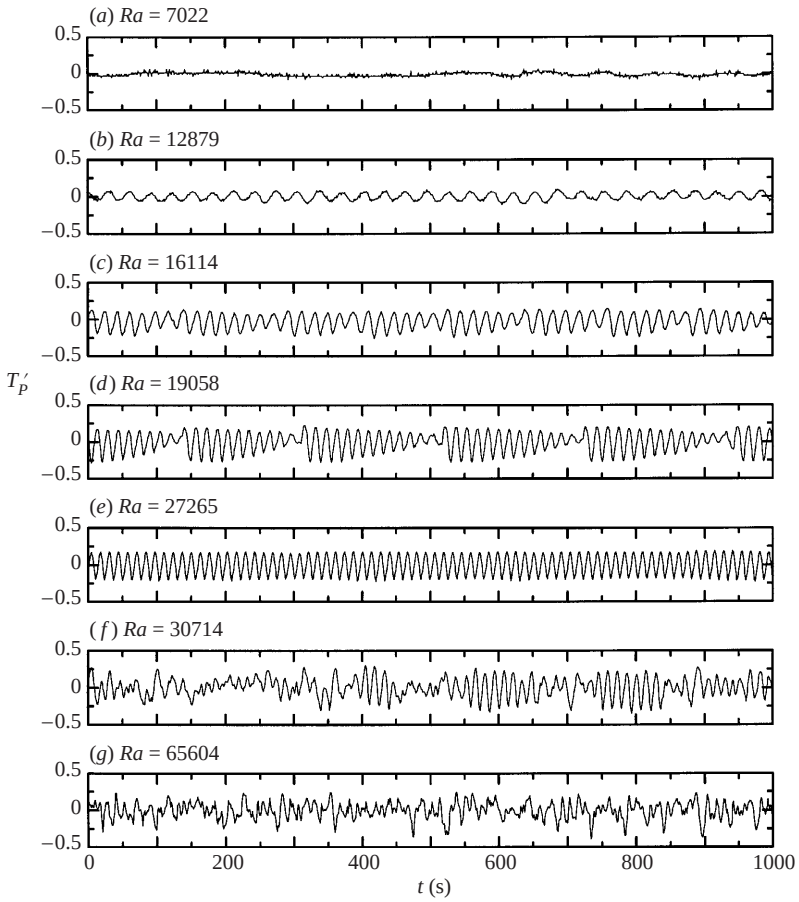

FIGURE 11. Time series of the dimensionless fluctuating part of temperature T_P' recorded by the probe for MHD flow at $M = 400$. The Rayleigh number is increased from a case of stationary flow shown in (*a*) to large supercritical conditions where time-dependent phenomena are dominant.

ratio and under the influence of a horizontal magnetic field have been investigated by Libchaber, Laroche & Fauve (1982) and Libchaber, Fauve & Laroche (1983). Their experiments were conducted for small intensities of the magnetic field and moderate supercritical Rayleigh numbers and under extremely well controlled thermal conditions. They observed highly ordered and complex oscillations with an ultimate transition to chaotic temporal behaviour.

In our experiments two sets of temperature time series are recorded: one for a fixed Hartmann number and varying Rayleigh number and the other for a fixed Rayleigh number and varying Hartmann number. In figure 11(*a*–*g*) time series of local temperature fluctuation T_P' at fixed Hartmann number $M = 400$ are displayed for increasing Rayleigh numbers. No significant fluctuations are observed for the lowest Rayleigh number $Ra = 7022$ (figure 11*a*) which is, according to table 1 and figure 6, a state just above the onset of convection. For increasing Rayleigh numbers regular temporal signals develop first. At $Ra = 12879$ (figure 11*b*) a quasi-harmonic signal is obtained which becomes modulated in a sawtooth manner at $Ra = 19058$ (figure 11*d*) on a time scale about 15 times longer than that of the basic oscillation. On increasing the Rayleigh number to $Ra = 27265$ (figure 11*e*) the fluctuation signal

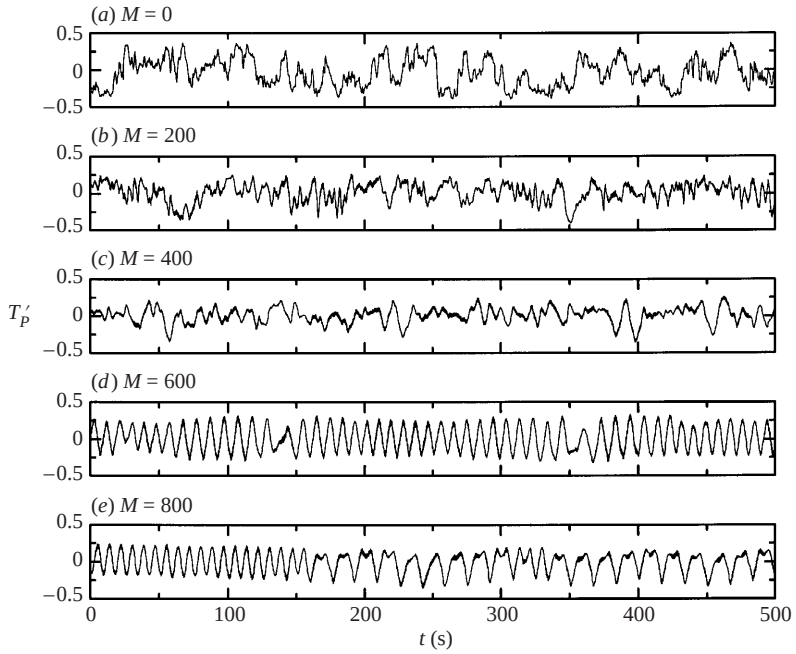

FIGURE 12. Temperature fluctuations T_P' recorded by the probe. At constant Rayleigh number $Ra = 5.0 \times 10^4$ the magnetic field is increased from OHD flow ($M = 0$) to MHD flows at Hartmann numbers $M = 200$, 400, 600 and 800.

returns to a mono-periodic, nearly harmonic behaviour. It is noteworthy that the intensity of these temperature fluctuations amounts to about 40% of the driving temperature difference across the layer and moreover that the periodic signal in figure 11(*e*) corresponds to the local maximum of the Nusselt number in figure 6. If the Rayleigh number is further increased, the regular temporal pattern disintegrates, developing intermittencies at $Ra = 30714$ (figure 11*f*) and finally chaotic and turbulent behaviour at $Ra = 65604$ (figure 11*g*). The transition of the convective flow from regular to chaotic temporal character is related to the drastic decrease of heat transfer as indicated by the drop in the Nusselt number in figure 6. This observation suggests that the heat transfer can be improved if the time-dependent flow becomes well ordered under the influence of an external controlled parameter, here the magnetic field.

In a second series of measurement long-term records ($t_m = 2^{14}$ s) of temperature time series are taken at a constant Rayleigh number $Ra = 5.0 \times 10^4$ for OHD flow with $M = 0$ and for MHD convection with Hartmann numbers $M = 200$, 400, 600 and 800. Parts of the time series are shown in figure 12. Starting from a chaotic signal for $M = 0$ the flow undergoes a transition to more regular behaviour until for $M = 600$ and 800 quasi-periodic temporal patterns appear, which for $M = 600$ show some intermittencies and for $M = 800$ a bimodal feature.

The transition from an irregular chaotic, say turbulent, temporal behaviour to an ordered quasi-periodic state is reflected well in the power density spectra of the recorded signals. The spectra evaluated for different magnetic fields are shown in figure 13. For OHD convection ($M = 0$) and for a weak magnetic field ($M = 200$) the power spectra show a monotonic decrease with increasing frequencies. For OHD convection the power decays in the high-frequency range like f^{-4}, which agrees with

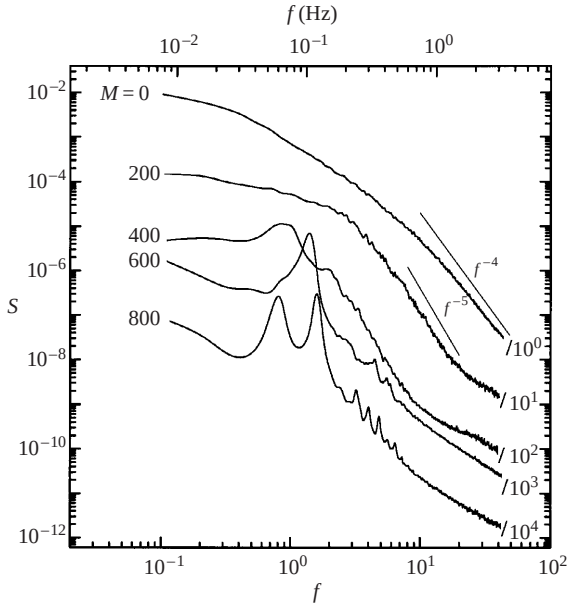

FIGURE 13. Phase-averaged energy spectra S of temperature fluctuations T_P' recorded by the probe at $Ra = 5.0 \times 10^5$. For the Hartmann numbers $M = 0$, 200, 400, 600 and 800 the Nusselt numbers $Nu = 2.06$, 1.70, 1.45, 1.72 and 1.38 are obtained. Each energy spectrum is rescaled by a constant factor given at the right-hand ends of the curves such that interlacing is reduced considerably.

the experimental findings of Horanyi *et al.* (1999) for Rayleigh–Bénard convection in liquid sodium layers. The decay becomes faster for the case of weak magnetic fields ($M = 200$ and 400), namely the power decays like f^{-5} in a frequency range of about $1 \lesssim f \lesssim 10$ which is explained by the additional Joule damping effect. The monotonic property of the power spectra is lost for even higher Hartmann numbers. As indicated by the local maxima the power spectra accumulate around certain frequencies and single and multiple peaks are observed. The number of identifiable frequencies seems to increase with increasing intensity of the magnetic field, indicating the emergence of well organized spatial structures in the convective flow.

Although the recordings of the embedded wall thermocouples (see figure 3) are limited in intensity and frequency range because of the conductive damping of the copper plate the power containing oscillations can be identified from the signal and used for spatial correlations. In figure 14 the recordings of temperature fluctuations of three thermocouples $T_{N,b}$, $T_{M,b}$ and $T_{S,b}$, embedded in the lower heated copper plate and the probe are displayed for a weak (figure 14*a*) and a strong (figure 14*b*) magnetic field intensity corresponding to $M = 200$ and 600 respectively. Notice that the three wall thermocouples form a line parallel to the applied magnetic field. For the weak field ($M = 200$) the signals are barely correlated whereas for the stronger field intensity ($M = 600$) the signals are very well correlated. This observation is expressed more precisely by the cross-correlation coefficients

$$K_{ij} = \frac{\overline{T_i' T_j'}}{\left(\overline{T_i'^2}\ \overline{T_j'^2}\right)^{1/2}} \tag{37}$$

which are listed in table 2.

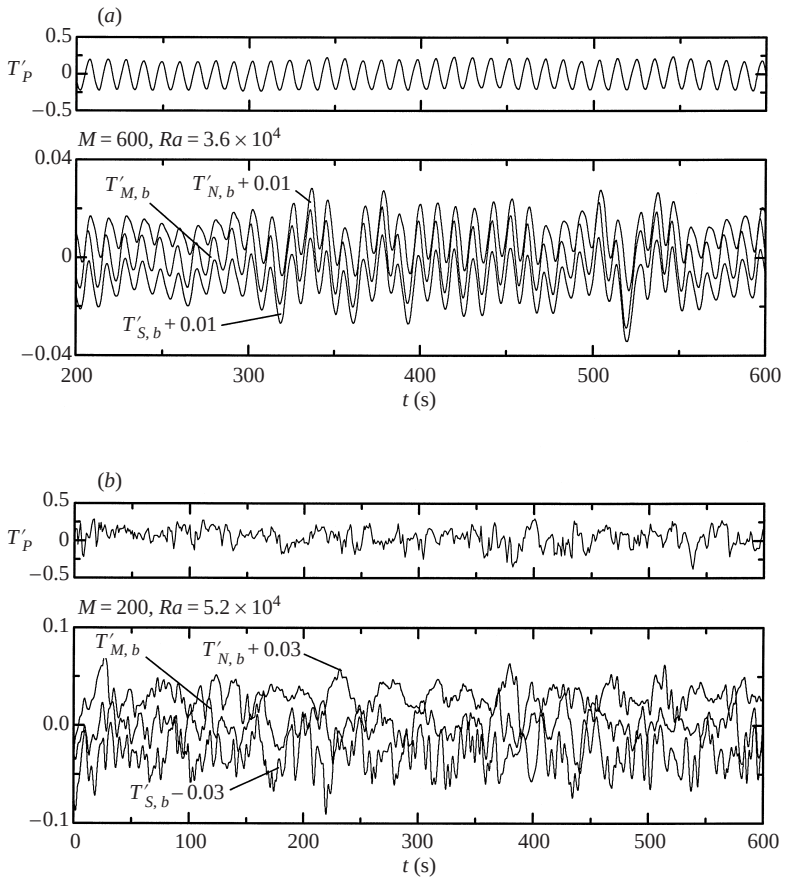

FIGURE 14. Comparison of the fluctuating parts of the temperature signal T'_P obtained from the probe (upper graphs) with fluctuating parts of the temperature signals obtained from three wall thermocouples $T_{N,b}$, $T_{M,b}$ and $T_{S,b}$ of the bottom wall (lower graphs). The three wall elements form a line parallel to the magnetic field (see figure 3). (*a*) $Ra = 3.6 \times 10^4$ and $M = 600$ and (*b*) $Ra = 5.2 \times 10^4$ and $M = 200$.

	$M = 600$, $Ra = 3.6 \times 10^4$				$M = 200$, $Ra = 5.2 \times 10^4$			
$K_{i,j}$	$T'_{N,b}$	$T'_{M,b}$	$T'_{S,b}$	T'_P	$T'_{N,b}$	$T'_{M,b}$	$T'_{S,b}$	T'_P
$T'_{N,b}$	1	0.794	0.872	0.022	1	0.019	0.046	−0.032
$T'_{M,b}$	0.794	1	0.967	0.021	0.019	1	0.386	−0.030
$T'_{S,b}$	0.872	0.967	1	0.024	0.046	0.386	1	−0.026
T'_P	0.022	0.021	0.024	1	−0.032	−0.030	−0.026	1

TABLE 2. Cross-correlation coefficients $K_{i,j}$ of temperature fluctuations as defined by equation (37) obtained from the wall thermocouples $T_{N,b}$, $T_{M,b}$ and $T_{S,b}$ and the probe T'_P for the same parameter combinations as given in figure 14.

Significantly lower values are obtained for the weaker magnetic field intensity ($M = 200$) which strongly support our conjecture that coherent two-dimensional spatial structures are established in the direction of a strong enough externally imposed horizontal magnetic field.

7. Concluding remarks

For high-intensity horizontal magnetic fields and under appropriate boundary conditions a liquid metal natural convective flow can be described by two-dimensional model equations that take into account Joule dissipation, caused by Hartmann braking at the walls perpendicular to the magnetic field, with a magnetic damping parameter $1/\tau$. The crucial condition for the validity of such a quasi-two-dimensional (Q2D) description of the flow is the requirement that the ratio between buoyant and electrodynamic forces is small, i.e. $Ra/Q \ll 1$. A linear stability analysis of the quasi-two-dimensional equations shows that the critical Rayleigh number for the onset of convection is shifted to significantly higher values. In the limiting case of negligible viscous dissipation the asymptotic law $Ra_c = 4\pi^2/\tau$ is valid. Experiments confirm the theoretical values for critical Rayleigh numbers with high accuracy in the case of strong magnetic fields ($Q \geqslant 400$); for weaker magnetic fields the theory overestimates the effect of magnetic damping and thus shows that the quasi-two-dimensional description is not valid generally. At supercritical conditions, the electrodynamic effects exert a significant influence on the convective heat transport. Consistent with the stabilizing effect the Nusselt numbers are in general significantly decreased by Joule dissipation. However, there are also regions of enhanced heat transfer surpassing even that of OHD convection. The local isotropy coefficients of the local temperature gradient measured by a probe in the midplane of the layer show that the increase of convective heat transport goes along with the transition of the convection pattern into an increasingly non-isotropic state of convection rolls predominantly aligned with the magnetic field. The increasing two-dimensionality generally reduces nonlinearities and the three-dimensional cascading process towards smaller scales is inhibited. Instead, large-scale convective vortices are formed and the temporal dynamics of the convective flow may become dominated by a few superimposed or even one single frequency. Because of both the reduced Joule dissipation of non-isotropic flow and the reduced viscous dissipation of the larger flow structures, convective velocities as well as the convective heat transport are increased.

From the comparison of temperature recordings of three wall thermocouples that are arranged in a line parallel to the magnetic field, the existence of coherent time-dependent quasi-two-dimensional flow over a distance of ten times the height of the layer is observed for strong magnetic fields and moderate Rayleigh numbers.

Although the intensity of temperature fluctuations at high supercritical Rayleigh numbers may reach high values, comparable to those of OHD flow, there exists a narrow range of stationary convection with significant convective heat transfer. This may be significant for an application of horizontal magnetic fields to controlling certain metallurgical processes such as crystal pulling from convecting melts.

The authors are grateful to Dr L. Barleon, Dr L. Bühler, Dr R. Stieglitz and Professor A. Tsinober for useful discussions and comments. Special thanks are due to Mr K.-J. Mack for his excellent technical assistance especially in running the superconducting magnet. All experiments have been performed in the MEKKA facility of the Institut für Angewandte Thermo- und Fluiddynamik of the Forschungszentrum Karlsruhe.

REFERENCES

Bühler, L. 1996 Instabilities in quasi-two-dimensional magnetohydrodynamic flows. *J. Fluid Mech.* **326**, 125–150.

Burr, U., Barleon, L., Müller, U. & Tsinober, A. 2000 Turbulent transport of momentum and

heat in magnetohydrodynamic rectangular duct flow with strong sidewall jets. *J. Fluid Mech.* **406**, 247–279.

Burr, U. & Müller, U. 2001 Rayleigh–Bénard-convection in liquid metal layers under the influence of a vertical magnetic field. *Phys. Fluids* **13**, 3247–3257.

Chandrasekhar, S. 1961 *Hydrodynamic and Hydromagnetic Stability*. Dover.

Davidson, P. A. 1995 Magnetic damping of jets and vortices. *J. Fluid Mech.* **299**, 153–186.

Fauve, S., Laroche, C. & Libchaber, A. 1981 Effect of a horizontal magnetic field on convective instabilities in mercury. *J. Physique-Lettres* **42**, L-455–L-457.

Fauve, S., Laroche, C., Libchaber, A. & Perrin, B. 1984 Chaotic phases and magnetic order in a convective fluid. *Phys. Rev. Lett.* **52**, L-211–L-216.

Foust, O. 1972 *Sodium-NaK Engineering Handbook*, Vol. 1. Gordon and Breach.

Horanyi, S., Krebs, L. & Müller, U. 1999 Turbulent Rayleigh–Bénard convection in low Prandtl-number fluids. *Intl J. Heat Mass Transfer* **42**, 3983–4003.

Horton, C. W. & Rogers, F. T. 1945 Convection currents in a porous medium. *J. Appl. Phys.* **16**, 367–370.

Kishida, Y. & Takeda, K. 1994 Suppression of turbulent Bénard convection by horizontal D.C. magnetic field. *Proc. Intl Symp. on Electromagnetic Processing of Materials, October 25–28, Nagoya, Japan, ISIJ* (ed. S. Asai), pp. 80–85. The Iron and Steel Institute of Japan.

Lapwood, E. R. 1941 Convection of a fluid in a porous medium. *Proc. Camb. Phil. Soc.* **44**, 508–521.

Lehnert, L. & Little, N. C. 1956 Experiments on the effect of inhomogeneity and obliquity of a magnetic field inhibiting convection. *Tellus* **9**, 97–103.

Libchaber, A., Fauve, S. & Laroche, C. 1983 Two parameter study of the route to chaos. *Physica* **7D**, 73–84.

Libchaber, A., Laroche, C. & Fauve, S. 1982 Period doubling cascade in mercury a quantitative measurement. *J. Physique-Lettres* **43**, L-211–L-216.

Lyon, R. N. 1952 *Liquid Metals Handbook*, 2nd edn. Washington, Atomic Energy Commission, Department of the Navy Washington, DC.

O'Donnell, J. O., Papanicolaou, P. G. & Reed, C. B. 1989 The thermophysical and transport properties of eutectic NaK near room temperature. *Tech. Rep.* Aragonne National Laboratory ANL/FPP/TM–237.

Rossby, H. 1969 A study of Bénard convection with and without rotation. *J. Fluid Mech.* **36**, 309–335.

Sommeria, J. & Moreau, R. 1982 Why, how and when, MHD turbulence becomes two-dimensional. *J. Fluid Mech.* **118**, 507–518.

Verron, J. & Sommeria, J. 1987 Numerical simulation of the two-dimensional turbulence experiment in magnetohydrodynamics. *Phys. Fluids* **30**, 732–739.

Walker, J. S. 1981 Magnetohydrodynamic duct flows in rectangular ducts with thin conducting walls I. *J. Méc.* **20**, 79–112.

Wesfreid, J., Pomeau, Y., Dubois, M., Normand, C. & Berge, P. 1978 Critical effects in Rayleigh–Bénard-convection. *Le Journal de Physique*, **39**, 725–731.